This article has been accepted for publication in a future issue of this journal, but has not been fully edited. Content may change prior to final publication. Citation information: DOI 10.1109/TAP.2022.3165540, IEEE Transactions on Antennas and Propagation

General Framework for Array Noise Analysis and Noise Performance of a Two-Element Interferometer with a Mutual-Coupling Canceler

Leonid Belostotski, *Senior Member, IEEE*, Adrian Sutinjo, *Senior Member, IEEE*, Ravi Subrahmanyan, Soumyajit Mandal, *Senior Member, IEEE*, and Arjuna Madanayake, *Member, IEEE*

***Abstract*—This paper investigates the noise performance of a two-element phased array and interferometer containing a recently introduced self-interference canceler, which in the context of this work acts as a mutual-coupling canceler. To this end, a general framework is proposed to permit noise analysis of this network and a large variety of other networks. The framework-based numerical analysis for a two-element phased array shows that the addition of the canceler significantly increases the beam-equivalent noise temperature. For a two-element interferometer used in cosmology, this increase in noise temperature is still acceptable as the sky noise temperature in the 20-to-200-MHz band is high. When used in an interferometer, the canceler provides the ability to null mutual coherence at the interferometer output. The ability to provide matching to reduce the sensitivity of the null in mutual coherence to the phase of the 90° hybrids in the canceler is discussed.**

***Index Terms*—Antenna arrays, noise coupling, coupling canceler**

I. Introduction

ANTENNA arrays are increasingly used in modern communication and remote-sensing systems, scientific instruments, military equipment, and biomedical devices [1]–[11]. In comparison to single-antenna transceivers, the design of antenna-array transceivers is challenging due to electromagnetic coupling between antennas [12], [13]. However, antenna arrays offer new opportunities, such as, for example, beam steering and noise shaping [14], [15]. Two-element arrays form an important subset of arrays that are both used on their own and also as tools for studying the performance of larger arrays on a smaller and tractable scale.

This paper investigates the impact of a recently introduced wideband self-interference canceler, which was originally aimed at full-duplex multiple-input multiple-output (MIMO) wireless systems [16] and is similar to an earlier work in [17]. The cancellation is based on replica antennas that are located in isolation within an electromagnetically shielded absorptive box. The replica antennas mimic mutual coupling and scattering of the main antennas, thus allowing passive microwave-based subtraction of coupled components from the signals of interest [16]. While an inspection of the canceler network suggests that this replica-antenna-based canceler is expected to increase the beam-equivalent noise temperature, T_{rec}, of such an array, the canceler provides the possibility of decoupling the antennas and thus has potential uses in radio cosmology.

Manuscript received on XXXX XX, 202X. This work was supported by the University of Calgary, the Natural Sciences and Engineering Research Council of Canada, Canada Reasearch Chair Program, and CMC Microsystems.

L. Belostotski is with the Department of Electrical and Software Engineering, University of Calgary (e-mail: lbelosto@ucalgary.ca).

A. Sutinjo is with the School of Elecrical Engineering, Computer and Math Science, Curtin University.

R. Subrahmanyan is with CSIRO Astronomy & Space Science, Kensington WA, Australia.

S. Mandal is with the Instrumentation Division at Brookhaven National Laboratory, New York.

A. Madanayake is with the Department of Electrical and Computer Engineering, Florida International University.

Radio cosmology instruments typically rely on interferometric measurements to discern 10s to 100s mK spectrally rich perturbations in the Cosmic Microwave Background of 3 K, that is itself much weaker than the Galactic noise of $\sim 10^2$ to 10^4 K. Fortunately, while Galactic signals are strong, their smooth spectra permit their separation from cosmological signals. A single-antenna radiometer has already been used for cosmology experiments between 50 and 100 MHz [18]. Interferometric instruments are now being investigated [19] to verify the outcomes of [18].

A cosmology interferometer is expected to consist of two closely spaced antennas connected to receiver circuitry followed by a correlator. The close antenna spacing ($< 0.4\lambda$, where λ is the wavelength) realizes correlation for isotropic noise of the surrounding medium [20] that is subsequently detected by the correlator for measuring the noise temperature of a uniform sky, T_{sky}. Design equations for such a system, without the decoupling network, were recently presented in [20], where it was shown that the cross-correlation does indeed contain the desired signal, particularly when the antenna spacing is minimized. However, the mutual coupling of closely spaced antennas results in the noise from each receiver propagating to the output through multiple paths, thereby contaminating the output by the undesirable mutual coherence. To reduce this contamination, a decoupling network may be employed [21]–[26]. While isolators form an intuitive implementation of such a network, their bandwidths are limited to approximately 10% in the 20-to-200-MHz frequency range. Instead, a wideband decoupling network stemming from the work in [16] is considered here. As is shown, this network is able to decouple antennas and thereby null the mutual-coupling-induced correlation in two-element interferometer-based cosmology instruments.

In Section II, we derive key equations that form a general framework for describing the noise performance of an M-element array. This framework is used in the rest of the paper, which is divided into two sections: Section III discusses the beam-equivalent noise temperature, T_{rec}, of the two-element array, and Section IV investigates the mutual coherence of the system. Finally, Section V discusses our results, and Section VI concludes the paper.

II. Antenna Array with the Canceler

The noise of antenna arrays directly connected to receivers has been investigated in the past by many groups [27]–[31]. These investigations have adopted different approaches to deriving expressions for noise analysis but they are all specific to their particular systems and are not applicable to the network discussed here. Therefore, we start by developing a general framework that can be adopted for any other network while also avoiding the need for manual error-prone signal-flow-graph analysis. We use this framework to analyze the noise behavior of the system shown in Fig. 1. This block diagram is a receiver-only implementation of the system based on [16]. The main array consists of the M-antenna array, labeled as Antenna #1 to #M, and referred to as "antenna array" in the rest of the paper. The replica array is nominally identical to the main array but placed

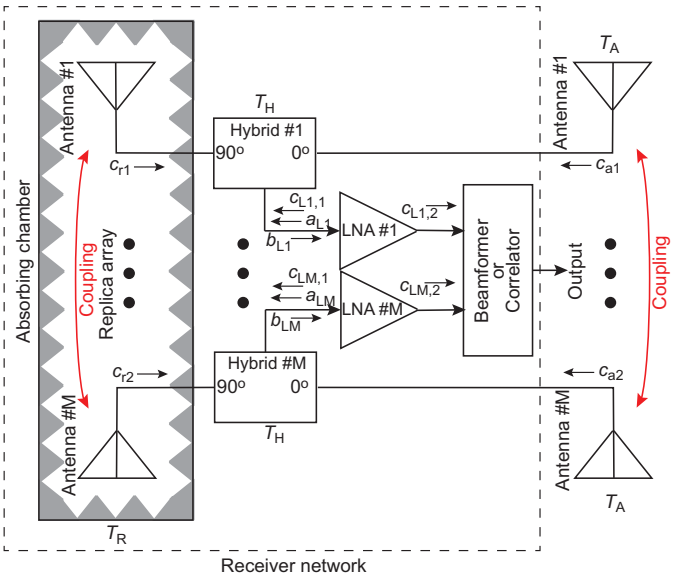

Fig. 1. Block diagram of an M-element array with the mutual-coupling canceler implemented with a replica array and 90° hybrids.

in an absorbing chamber. Unlike [16], two nominally identical 90° hybrids are used. In addition to preserving the cancellation property analyzed in [16], these hybrids have two advantages: the reflection coefficients as seen by the LNAs only depend on the hybrid and do not depend on the antenna array, and maintaining similar performance between two 90° hybrids is easier than between the splitter and 180° hybrid used in the system in [16]. The receiver network, as identified in the figure, consists of the replica array, hybrids, LNAs, and a beamformer or correlator. The noise of the complete system is modeled by noise waves $\mathbf{c}$ emanating out of input and output ports of all sub-components. In a conventional implementation, i.e. without the replica array and the hybrids, the noise emanating from the LNA inputs, such as $c_{\mathrm{L}1,1}$ to $c_{\mathrm{LM},1}$, couples to adjacent antennas and propagates to the beamformer. Such coupling causes non-zero cross correlation [20]. With the replica array in place, $c_{\mathrm{L}i,1}$, where $i = 1 \ldots M$, propagate to the beamformer through two paths while experiencing a 180° phase shift, thus providing the possibility of cancellation. While cancellation of coupled $c_{\mathrm{L}i,1}$ is therefore possible, the additional absorbing chamber and hybrids undoubtedly contribute additional noise.

A. Key Equations

A set of linear equations that relate traveling waves at the ports of the complete network is

$$\mathbf{b} = \mathbf{S}\left(\mathbf{a} + \mathbf{a}_{\mathrm{s}}\right) + \mathbf{c} \tag{1}$$

with

$$\mathbf{S} = \begin{bmatrix} \mathbf{S}_{\mathrm{PASS}} & \mathbf{0} \\ \mathbf{0} & \mathbf{S}_{\mathrm{ACT}} \end{bmatrix} \tag{2}$$

where in general $\mathbf{S}_{\mathrm{PASS}}$ and $\mathbf{S}_{\mathrm{ACT}}$ are S-parameter matrices of the passive and active sub-circuits, respectively; $\mathbf{a}$ is a vector of all incident waves; $\mathbf{b}$ is a vector of all reflected waves; $\mathbf{a}_{\mathrm{s}}$ is a vector of generated waves of sources connected to the network ports; and the noise waves are represented by the vector $\mathbf{c}$.

The connections between all internally interconnected ports in the system are identified by $\mathbf{K}$, where $\mathbf{a} = \mathbf{K}\mathbf{b}$, such that (1) becomes

$$\mathbf{b} = \mathbf{S}\left(\mathbf{K}\mathbf{b} + \mathbf{a}_{\mathrm{s}}\right) + \mathbf{c} \tag{3}$$

and forms the main expression that is used throughout this work to determine the noise and gain of the system.

Whereas (1) to (3) are general, for the particular system in Fig. 1, the elements of (1) and (2) are

$$\mathbf{S}_{\mathrm{PASS}} = \begin{bmatrix} \mathbf{S}_{\mathrm{A}_{M\times M}} & & & \\ & \mathbf{S}_{\mathrm{R}_{M\times M}} & & \mathbf{0} \\ & & \mathbf{S}_{\mathrm{H1}_{3\times 3}} & \\ & \mathbf{0} & & \ddots \\ & & & \mathbf{S}_{\mathrm{HM}_{3\times 3}} \end{bmatrix}, \tag{4}$$

$$\mathbf{S}_{\mathrm{ACT}} = \begin{bmatrix} \mathbf{S}_{\mathrm{L1}_{2\times 2}} & & \mathbf{0} \\ & \ddots & \\ \mathbf{0} & & \mathbf{S}_{\mathrm{LM}_{2\times 2}} \end{bmatrix}, \tag{5}$$

$$\begin{aligned} \mathbf{a} &= \begin{bmatrix} \mathbf{a}_{\mathrm{A}} & \mathbf{a}_{\mathrm{R}} & \mathbf{a}_{\mathrm{H}} & \mathbf{a}_{\mathrm{L}} \end{bmatrix}^T_{1\times 7M}, \\ \mathbf{b} &= \begin{bmatrix} \mathbf{b}_{\mathrm{A}} & \mathbf{b}_{\mathrm{R}} & \mathbf{b}_{\mathrm{H}} & \mathbf{b}_{\mathrm{L}} \end{bmatrix}^T_{1\times 7M}, \\ \mathbf{c} &= \begin{bmatrix} \mathbf{c}_{\mathrm{A}} & \mathbf{c}_{\mathrm{R}} & \mathbf{c}_{\mathrm{H1}} & \mathbf{c}_{\mathrm{H2}} & \mathbf{c}_{\mathrm{L1}} & \mathbf{c}_{\mathrm{L2}} \end{bmatrix}^T_{1\times 7M} \\ &= \begin{bmatrix} \mathbf{c}_{\mathrm{PASS}} & \mathbf{c}_{\mathrm{ACT}} \end{bmatrix}^T, \end{aligned} \tag{6}$$

where subscripts A, R, H1(2), and L1(2) identify the antenna array, replica array, hybrids #1(#2), and LNAs #1(#2), respectively. The vector $\mathbf{c}$ consists of individual noise contributions from each passive and active parts of the antenna network. For a two-antenna system, $\mathbf{c}_{\mathrm{A}} = \begin{bmatrix} c_{\mathrm{a}1} & c_{\mathrm{a}2} \end{bmatrix}$, $\mathbf{c}_{\mathrm{R}} = \begin{bmatrix} c_{\mathrm{r}1} & c_{\mathrm{r}2} \end{bmatrix}$, $\mathbf{c}_{\mathrm{H1}} = \begin{bmatrix} c_{\mathrm{h}1,1} & c_{\mathrm{h}1,2} & c_{\mathrm{h}1,3} \end{bmatrix}$, $\mathbf{c}_{\mathrm{H2}} = \begin{bmatrix} c_{\mathrm{h}2,1} & c_{\mathrm{h}2,2} & c_{\mathrm{h}2,3} \end{bmatrix}$, $\mathbf{c}_{\mathrm{L1}} = \begin{bmatrix} c_{\mathrm{L}1,1} & c_{\mathrm{L}1,2} \end{bmatrix}$, and $\mathbf{c}_{\mathrm{L2}} = \begin{bmatrix} c_{\mathrm{L}2,1} & c_{\mathrm{L}2,2} \end{bmatrix}$. If required, matrix $\mathbf{S}$ in (4) can also include S-parameters of the beamformer/correlator to account for any impedance mismatch at the correlator/beamformer input and its gain. Note that (4) assumes a 3-port S-parameter model of hybrids. In the situations when hybrids are 4-port devices requiring a matched load at the extra port, S_{H} becomes a 4-port matrix in (4). In this case S_{PASS} would also include 1-port S-parameter matrices for each termination.

B. Noise

For noise analysis, the input signals are removed by setting $\mathbf{a}_{\mathrm{s}} = [\mathbf{0}]$, and the noise waves, $\mathbf{b}_{\mathrm{n}}$, emanating from each port of the network are found from (3) as

$$\mathbf{b}|_{\mathbf{a}_{\mathrm{s}}=[\mathbf{0}]} \equiv \mathbf{b}_{\mathrm{n}} = \left(\mathbf{I} - \mathbf{S}\mathbf{K}\right)^{-1}\mathbf{c} = \mathbf{Q}\mathbf{c}, \tag{7}$$

where $\mathbf{Q}$ is introduced for brevity and $\mathbf{I}$ is the identify matrix. The noise-correlation matrix is described by

$$\overline{\mathbf{b}_{\mathrm{n}}\mathbf{b}_{\mathrm{n}}^{\dagger}} = \mathbf{Q}\overline{\mathbf{c}\mathbf{c}^{\dagger}}\mathbf{Q}^{\dagger} \tag{8}$$

where "†" indicates a Hermitian conjugate operator and, for the passive components, the terms of $\overline{\mathbf{c}\mathbf{c}^{\dagger}}$ are found from Bosma's theorem [32], [33] as

$$\overline{\mathbf{c}_{\mathrm{PASS}}\mathbf{c}_{\mathrm{PASS}}^{\dagger}} = kB\left(\mathbf{I} - \mathbf{S}_{\mathrm{PASS}}\mathbf{S}_{\mathrm{PASS}}^{\dagger}\right)\mathbf{T}_{\mathrm{PASS}}, \tag{9}$$

where $\mathbf{T}_{\mathrm{PASS}}$ is the diagonal matrix of the physical temperatures of all passive components. $\mathbf{T}_{\mathrm{PASS}}$ is a $5M \times 5M$ matrix for the system in Fig. 1. Assuming that the LNAs are identical (i.e., noise-correlation matrices $\overline{\mathbf{c}_{\mathrm{L1}}\mathbf{c}_{\mathrm{L1}}^{\dagger}} = \ldots = \overline{\mathbf{c}_{\mathrm{LM}}\mathbf{c}_{\mathrm{LM}}^{\dagger}} = \mathbf{c}_{\mathrm{L}}$), the terms in $\overline{\mathbf{c}\mathbf{c}^{\dagger}}$ due to active components (i.e. $\overline{\mathbf{c}_{\mathrm{ACT}}\mathbf{c}_{\mathrm{ACT}}^{\dagger}}$) are found from active component noise parameters [34, p. 54] as

$$\mathbf{c}_{\mathrm{L}} = kT_{\mathrm{L}}B\begin{bmatrix} \overline{|c_{\mathrm{L},1}|^2} & \overline{c_{\mathrm{L},1}c_{\mathrm{L},2}^{*}} \\ \overline{c_{\mathrm{L},1}^{*}c_{\mathrm{L},2}} & \overline{|c_{\mathrm{L},2}|^2} \end{bmatrix} \tag{10}$$

where $T_{\mathbf{L}}$ is the LNA physical temperature[1] and

$$\begin{cases} \overline{|c_{\mathrm{L},1}|^2} = \frac{T_{min}}{T_0}\left(|S_{\mathrm{L},11}|^2-1\right)+4N\frac{\left|1-S_{\mathrm{L},11}\Gamma_{opt}\right|^2}{1-\left|\Gamma_{opt}\right|^2} \\ \overline{|c_{\mathrm{L},2}|^2} = |S_{L,21}|^2\left(\frac{T_{min}}{T_0}+4N\frac{|\Gamma_{opt}|^2}{1-\left|\Gamma_{opt}\right|^2}\right) \\ \overline{c_{\mathrm{L},1}c^*_{\mathrm{L},2}} = \frac{S_{\mathrm{L},11}}{S_{\mathrm{L},21}}\overline{|c_{\mathrm{L},2}|^2}-4N\frac{S^*_{\mathrm{L},21}\Gamma^*_{opt}}{1-\left|\Gamma_{opt}\right|^2}. \end{cases} \tag{11}$$

The noise parameters in (11) are: the minimum noise temperature, T_{min}; the Lange invariant, N [35], [36]; and the optimum reflection coefficient for minimum noise, Γ_{opt}.

Having found $\overline{\mathbf{b}_{\mathrm{n}}\mathbf{b}_{\mathrm{n}}^\dagger}$ in (8), we can calculate beam-equivalent receiver noise temperature, T_{rec}, with [37], [38]

$$T_{\mathrm{rec}} = T_0\frac{\tilde{\mathbf{w}}^\dagger\left.\overline{\mathbf{b}_{\mathrm{n}}\mathbf{b}_{\mathrm{n}}^\dagger}\right|_{T_{\mathrm{A}}=0}\tilde{\mathbf{w}}}{\tilde{\mathbf{w}}^\dagger\left.\overline{\mathbf{b}_{\mathrm{n}}\mathbf{b}_{\mathrm{n}}^\dagger}\right|_{\text{only } T_{\mathrm{A}}\neq 0}\tilde{\mathbf{w}}}, \tag{12}$$

where $\tilde{\mathbf{w}}$ is the vector of complex gains of the beamformer/correlator in which all terms are zero except for those pertaining to the elements of $\mathbf{b}$ that relate to power flow to the beamformer/correlator. The beam-equivalent noise temperature T_{rec} is defined with reference to the response of the antenna arrays to an isotropic external noise environment at temperature T_0 with which they are in thermal equilibrium.

Further, we find the cross-correlation between outputs i and j in the form of noise temperature by

$$T_{ij} = \frac{1}{kB}\tilde{\mathbf{w}}_i^\dagger\left.\overline{\mathbf{b}_{\mathrm{n}}\mathbf{b}_{\mathrm{n}}^\dagger}\right|_{\mathbf{a}_{\mathrm{s}}=[\mathbf{0}]}\tilde{\mathbf{w}}_j. \tag{13}$$

C. Gain

To find gain, we set $\mathbf{c} = [\mathbf{0}]$ and set $\mathbf{a}_{\mathrm{s}}$ elements, which correspond to the antenna-array ports, non-zero to apply source waves at the outputs of array antennas in (3) to obtain

$$\mathbf{b} = \mathbf{QS}\mathbf{a}_{\mathrm{s}}. \tag{14}$$

With $\mathbf{b}$ from (14), in general the gain of the system in response to an input is

$$G = \frac{\tilde{\mathbf{w}}^\dagger\overline{\mathbf{b}\mathbf{b}^\dagger}\tilde{\mathbf{w}}}{\delta^\dagger\overline{\mathbf{a}_{\mathrm{s}}\mathbf{a}_{\mathrm{s}}^\dagger}\delta}, \tag{15}$$

where δ is the vector with non-zero terms pertaining to the array inputs. This gain definition considers any or all elements of $\mathbf{a}_{\mathrm{s}}$ as inputs and any or all elements of $\mathbf{b}$ as outputs. In practice, δ and $\mathbf{w}$ would only specify some of their elements, such as those pertaining to antenna ports as inputs and those pertaining to the waves traveling towards the beamformer as outputs. Further, the expression of the correlation gain can be obtained from (15) with

$$G_{ij} = \frac{\tilde{\mathbf{w}}_i^\dagger\overline{\mathbf{b}\mathbf{b}^\dagger}\tilde{\mathbf{w}}_j}{\delta_k^\dagger\overline{\mathbf{a}_{\mathrm{s}}\mathbf{a}_{\mathrm{s}}^\dagger}\delta_l^\dagger}, \tag{16}$$

where subscripts k and $l = 1\ldots M$ indicate elements of input vector $\mathbf{a}_{\mathrm{s}}$ that form the input to the system, and subscripts i and $j = 1\ldots M$ indicate outputs pertaining to the correlation gain of interest.

III. Two-Element Phased-Array T_{REC}

Conventionally, increasing array sensitivity requires the development of receivers such that their optimum reflection coefficient, $\Gamma_{\mathrm{opt}} \in \mathbb{C}$, for minimum noise equals the active reflection coefficient, $\Gamma_{\mathrm{act}} \in \mathbb{C}$, of the array [27]–[29], [37], [39]. For a given receiver, this equality can only be achieved for one scan angle, which results in only one beam whose noise can be fully minimized. For other scan angles, Γ_{act} deviates from Γ_{opt}, thereby increasing array noise above its minimum. The scan-dependence of Γ_{act} is due to mutual coupling of antennas in the array. Because of such coupling, some of the receiver noise couples to adjacent antennas and flows to the output through the beamformer, adversely impacting the output noise levels. Past methods of reducing mutual coupling included decoupling networks and low scattering antennas [21]–[25]. The authors of [26] demonstrated that decoupling is necessary for optimum noise matching of antenna arrays. Predictably, the addition of the decoupling network introduces noise, thus potentially negating the advantage of having a decoupled array.

In this section, we investigate the effect of the broadband mutual-coupling canceler on T_{rec} of a two-element antenna array and the possibility of using this canceler for making Γ_{act} scan independent.

A. Circuit models

In the following numerical calculations, we assume LNA $T_{\mathrm{min}} = 25\,\mathrm{K}$, $N = 0.03$, and $\Gamma_{\mathrm{opt}} = 0.2\angle 100^\circ$. Because both T_{min} and N are invariant upon lossless embedding, Γ_{opt} can be varied with a matching network without affecting T_{min} and N. We will use this fact to search for the optimum Γ_{opt} that minimizes T_{rec}. The S-parameters of the LNA are assumed as

$$\mathbf{S}_{\mathrm{L}} = \begin{bmatrix} 0.2\angle -75^\circ & 0.01\angle 150^\circ \\ 3\angle -150^\circ & 0.3\angle -100^\circ \end{bmatrix}. \tag{17}$$

We based the antenna array S-parameters on a scaled version of a 30-mm spaced two-element array described in [40]:

$$\mathbf{S}_{\mathrm{A}} = \mathbf{S}_{\mathrm{R}} = \begin{bmatrix} 0.3\angle 100^\circ & 0.2\angle -60^\circ \\ 0.2\angle -60^\circ & 0.3\angle 100^\circ \end{bmatrix}. \tag{18}$$

The ideal hybrid S-parameters are

$$\mathbf{S}_{\mathrm{H}} = \frac{1}{\sqrt{2}}\begin{bmatrix} 0 & 1\angle P_{\mathrm{H}} & 1 \\ 1\angle P_{\mathrm{H}} & 0 & 0 \\ 1 & 0 & 0 \end{bmatrix}, \tag{19}$$

where $P_{\mathrm{H}} = 90^\circ$, port 1 is the common port and ports 2 and 3 are the 90° and 0° coupled ports. For calculations with a non-ideal hybrid we use the manufacturer-specified S-parameters of a commercial component (Mini-Circuits JSPQW-100A+) at 100 MHz.

B. Numerical results

We first start with an ideal model in which we set LNA $\Gamma_{\mathrm{opt}} = 0$ and $S_{L,11} = 0$, use ideal hybrids, and sweep their phase P_{H} from 0° to 180° while keeping the physical temperatures of the antenna array and the LNA at 290 K and all other temperatures in $\mathbf{T}_{\mathrm{PASS}}$ at zero. The outcome of this baseline calculation is shown in Fig. 2(a). As can be seen, $P_{\mathrm{H}} = 90^\circ$ does indeed reduce T_{rec} as expected because mutual coupling between antennas is canceled. We also observe that the minimum T_{rec} is slightly higher than $2T_{\mathrm{min}}$. This is due to hybrid loss, L_{H}, and the impedance mismatch between the antenna and the hybrid. As a result, the variation of T_{rec} with P_{H} is very insignificant. When $S_{\mathrm{L},11}$ is set to its value in (17), the resultant T_{rec} remains unchanged as shown in Fig. 2(b).

Next, we assigned $\Gamma_{\mathrm{opt}} = 0.2\angle -100^\circ$ while keeping everything else unchanged. Fig. 2(c) shows that $P_{\mathrm{H}} = 90^\circ$ is no longer optimum. Instead, $P_{\mathrm{H}} \approx 17.5^\circ$ now realizes low T_{rec}. At $P_{\mathrm{H}} \approx 17.5^\circ$, mutual coupling is not canceled and beamformer dependent T_{rec} results. However, T_{rec} is reduced slightly from that in Figs. 2(a) and (b) demonstrating that the removal of mutual coupling is not necessarily required for improving the overall noise of the receiver under investigation.

[1]The assumption here is that the amplifier noise is linearly proportional to temperature around T_0= 290 K.

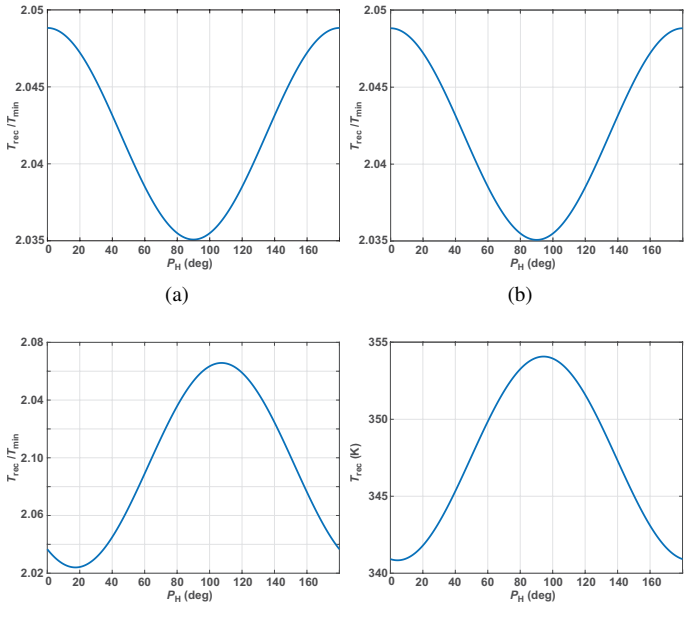

Fig. 2. T_{rec} for the system configured as: a) $\Gamma_{\text{opt}} = 0$, $S_{\text{L},11} = 0$, ideal hybrids, and $T_{\text{H}} = T_{\text{R}} = 0\,\text{K}$; b) Same as a) but with $S_{\text{L},11} = 0.2\angle -75°$; c) Same as b) but $\Gamma_{\text{opt}} = 0.2\angle -100°$; and d) same as c) but with all temperatures in $\mathbf{T}_{\text{PASS}}$ set to 290 K. Since in subfigure d) T_{rec} is dominated by the ambient temperature rather than T_{min}, the y-axis is not normalized.

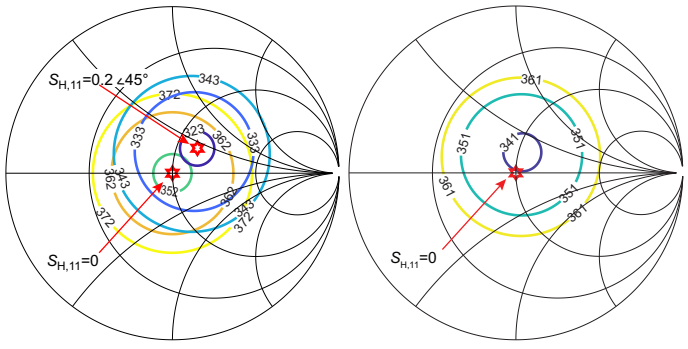

Fig. 3. Contours of constant T_{rec} as functions of Γ_{opt} at: a) $P_{\text{H}} = 90°$ for $S_{\text{H},11} = 0$ and $0.2\angle 45°$; and b) $P_{\text{H}} = 4.4°$ from 2(d) and for $S_{\text{H},11} = 0$.

Fig. 2(d) plots T_{rec} when temperatures of all components are set to 290 K. In this case, the replica array with the hybrids contributes 290 K in addition to $\sim L_{\text{H}} \times T_{\text{min}}$ from the LNA. As shown in these calculations, T_{rec} is significantly higher than T_{min}, and, therefore, from the array sensitivity point of view, this type of canceler network does not provide the benefits of high sensitivity. Based on this analysis and the general expectation that the replica array contributes T_{R} to T_{rec}, T_{rec} cannot be less than T_{R} even if the hybrids are designed such that $L_{\text{H}} = 0\,\text{dB}$. Comparing Figs. 2(c) and (d) suggests that in order to maintain T_{rec} between T_{min} and $L_{\text{H}}T_{\text{min}}$, the passives should be cooled to temperature much lower than 290 K. Reducing L_{H} would further help reducing T_{rec}.

In subsequent calculations, we set $P_{\text{H}} = 90°$ to investigate the independence of optimum Γ_{opt} on the values of beamformer coefficients. As shown by the contours of constant noise temperature in Fig. 3(a), the value of Γ_{opt} that exhibits the lowest T_{rec} coincides with $S_{\text{H},11}$ for two different values of $S_{\text{H},11}$: $S_{\text{H},11} = 0$ and $S_{\text{H},11} = 0.2\angle 45°$. Similar calculations show that the lowest T_{rec} always occurs when $\Gamma_{\text{opt}} = S_{\text{H},11}$ for any scan angle, i.e.

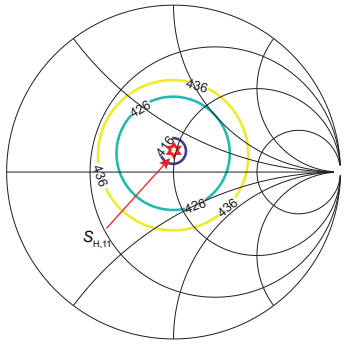

Fig. 4. Contours of constant T_{rec} as function of Γ_{opt} of the network with the non-ideal hybrid.

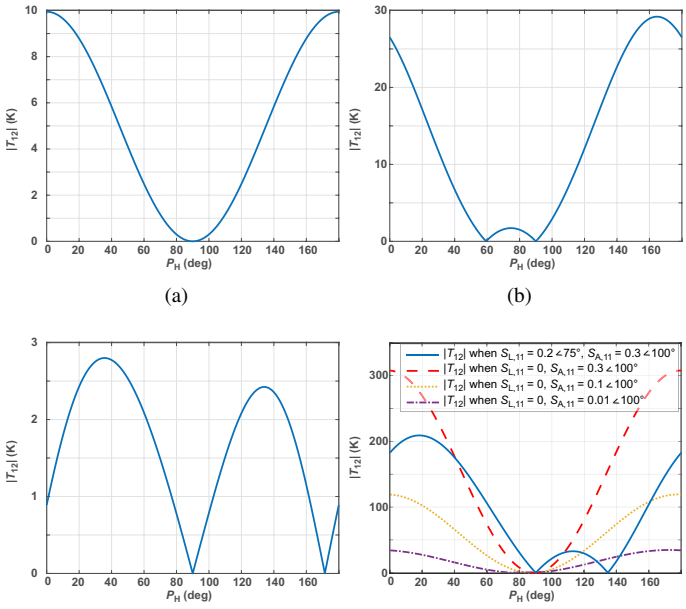

Fig. 5. $|T_{12}|$ for the system configured as: a) $\Gamma_{\text{opt}} = 0$, $S_{\text{L},11} = 0$, ideal hybrids, and $T_{\text{A}} = T_{\text{H}} = T_{\text{R}} = 0\,\text{K}$; b) Same as a) but with $S_{\text{L},11} = 0.2\angle -75°$; c) Same as b) but $\Gamma_{\text{opt}} = 0.2\angle -100°$; and d) same as c) but with all temperatures in $\mathbf{T}_{\text{PASS}}$ set to 290 K with two different setting for $S_{\text{L},11}$.

$\Gamma_{\text{act}} = S_{\text{H},11}$. It is important to note that while Γ_{act} is scan-angle independent, T_{rec} does depend on the scan angle when the reflection coefficients of antennas are not zero. When $P_{\text{H}} = 4.4°$ is selected from Fig. 2(d) to minimize T_{rec}, the optimum $\Gamma_{\text{opt}} \neq S_{\text{H},11}$, as seen from Fig. 3(b), and the array is no longer decoupled.

In the last step of this section, we replace the S-parameters of the ideal hybrid with the 100-MHz S-parameters of the commercial hybrid (Mini-Circuits JSPQW-100A+) . The outcome of this calculation in Fig. 4 shows the minimum of T_{rec} higher than in Fig. 3 due to the non-ideal hybrid while the network remains decoupled, and $\Gamma_{\text{opt}} = S_{\text{H},11}$ still minimizes T_{rec}.

IV. Two-Element Mutual Coherence

A. Single-Frequency Two-Element Interferometer

1) Ideal Hybrids: In this section, we reuse the same calculation setup as in Fig. 2 and determine the mutual coherence, in terms of $|T_{12}|$, of the two-element array with circuit components as in Section III-A. Fig. 5 shows the results of this numerical analysis.

As can be seen from the sub-figures, it is possible to adjust the phase of hybrids to reduce cross correlation to zero. As expected, $P_{\text{H}} = 90°$ is optimum, see Fig. 5. However, Fig. 5(b)

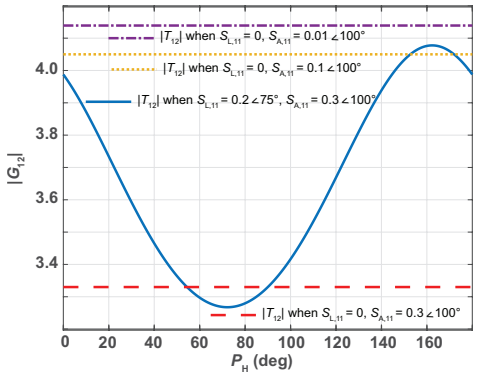

Fig. 6. Magnitude of correlation gain, $|G_{12}|$, (linear units) as a function of P_{H} for different $S_{\mathrm{L},11}$ and $S_{\mathrm{A},11(22)}$.

shows that due to non-zero $S_{\mathrm{L},11}$ a null in the cross-correlation also exists at $P_{\mathrm{H}} \approx 60^{\circ}$. The appearance of the second null can be explained with the following gedankenexperiment. Each LNA generates noise at both inputs, I_1 and I_2, to the cross correlator. The noise contributions of LNA#1 and LNA#2 to I_1 are denoted by uncorrelated $s_{1,1}$ and $s_{2,1}$, respectively, and their contributions to I_2 are denoted by uncorrelated $s_{1,2}$ and $s_{2,2}$. The output of the correlator is $\overline{I_1^* I_2} = \left(s_{1,1} + s_{2,1}\right)^* \left(s_{1,2} + s_{2,2}\right)$, which is equivalent to $\overline{I_1^* I_2} = \overline{s_{1,1}^* s_{1,2}} + \overline{s_{1,1}^* s_{2,2}} + \overline{s_{2,1}^* s_{1,2}} + \overline{s_{2,1}^* s_{2,2}}$, where the first term, pertaining to the noise of LNA#1, and the last terms, pertaining to LNA#2, are not zero. The other two terms are cross-correlations of LNA#1 and LNA#2 generated noise and therefore are zero. The locations of the two LNAs relative to I_1 and I_2 are different. It is expected that since for identical LNAs $\overline{s_{1,1}^* s_{1,2}} = \overline{s_{2,1} s_{2,2}^*}$, then $\overline{I_1^* I_2} = 2\Re\left\{\overline{s_{1,1}^* s_{1,2}}\right\}$, and it is possible to null the cross correlation by arranging P_{H} such that $\overline{s_{1,1}^* s_{1,2}}$ is purely imaginary. At $P_{\mathrm{H}} \approx 60^{\circ}$, $\overline{s_{1,1}^* s_{1,2}}$ is in fact purely imaginary causing low cross correlation. While the decoupling at $P_{\mathrm{H}} = 90^{\circ}$ due to hybrids is unique to the described system, the extra null in mutual coherence at $P_{\mathrm{H}} \approx 60^{\circ}$ is not unique and, for example, is present in (11) from [20].

Γ_{opt} is also responsible for moving the location of the additional null as can be seen by comparing Figs. 5(b) and (c). Further, having other system components contribute noise modifies the location of the extra null. The resultant P_{H} is dependent on $S_{\mathrm{L},11}$ and $S_{\mathrm{A},11(22)}$ as demonstrated in Fig. 5(d). As $S_{\mathrm{A},11(22)}$ approaches zero, the maximum of $|T_{12}|$ reduces because noise waves emanating from matched array ports connected to ideal hybrids exhibit no cross-correlation. However, the extra null still exists in this case albeit it is not very visible in the figure. Moreover, the array mutual coupling affects $|T_{12}|$. As the amount of coupling increases the peaks of the cross correlation function increase. Finally, these simulations show that a well-matched LNA with $|S_{\mathrm{L},11}| \approx 0$ avoids sharp nulls in $|T_{12}|$ and creates a smooth trough instead thereby reducing the sensitivity of $|T_{12}|$ to P_{H}.

Based on the same model settings as in Fig. 2(d), Fig. 6 also confirms that the correlation gain, G_{12}, of the network to a correlated input signal is not zero even at P_{H} where receiver-network-noise cross-correlation is nulled. To generate the input signal for this analysis, we make use of the results in [41], which showed that noise correlation matrix of an array due to thermal radiation from the warm scene can be found via Bosma's theorem. Therefore, to find G_{12}, the array is excited with an input $\mathbf{a}_{\mathrm{s}}$ whose noise-correlation matrix $\overline{\mathbf{a}_{\mathrm{s}}\mathbf{a}_{\mathrm{s}}^{\dagger}} = \begin{bmatrix} \overline{\mathbf{c}_{\mathrm{PASS}}\mathbf{c}_{\mathrm{PASS}}^{\dagger}} & \\ & \overline{\mathbf{c}_{\mathrm{L}}\mathbf{c}_{\mathrm{L}}^{\dagger}} \end{bmatrix}$. We set $T_{\mathrm{R}} = T_{\mathrm{H}} = T_{\mathrm{L}} = 0$. By doing so, only the antenna array excites the network, and other network components are prevented from adding to the output power of the interferometer and inadvertently increasing the computed gain. As the result $\overline{\mathbf{a}_{\mathrm{s}}\mathbf{a}_{\mathrm{s}}^{\dagger}} = \begin{bmatrix} \overline{\mathbf{c}_{\mathrm{A}}\mathbf{c}_{\mathrm{A}}^{\dagger}} & \mathbf{0} \end{bmatrix}$, and the correlation of the input signal received by the array is captured through the cross-correlation terms of $\mathbf{a}_{\mathrm{s}}\mathbf{a}_{\mathrm{s}}^{\dagger}$. While there is some phase dependence due to $S_{\mathrm{L},11}$, the gain G_{12}, as found from (16), remains non-zero and approximately near $|S_{\mathrm{L},21}|^2 / L_{\mathrm{H}}$ for all P_{H}. As $\left|S_{\mathrm{A},11(22)}\right|$ decreases the hybrid insertion loss decreases towards its minimum value of 2, thereby increasing G_{12} until its maximum value.

While the correlated noise from the replica array is canceled, $G_{12} \neq 0$ for the correlated output from the antenna array. To explain this, we consider a situation in which both arrays are placed in separate absorbing chambers at thermal equilibrium with all other passive components such that $T_{\mathrm{A}} = T_{\mathrm{R}} = T_{\mathrm{H}}$. In this case, the noises at the hybrid outputs are uncorrelated. If we now remove the absorbing chamber surrounding the antenna array, $\overline{\mathbf{c}_{\mathrm{A}}\mathbf{c}_{\mathrm{A}}^{\dagger}}$ changes from $\overline{\mathbf{c}_{\mathrm{A}}\mathbf{c}_{\mathrm{A}}^{\dagger}} = kB\left(\mathbf{I} - \mathbf{S}_{\mathrm{A}}\mathbf{S}_{\mathrm{A}}^{\dagger}\right)\mathbf{T}_{\mathrm{A}}$ to $\left[kB\left(\mathbf{I} - \mathbf{S}_{\mathrm{A}}\mathbf{S}_{\mathrm{A}}^{\dagger}\right)\mathbf{T}_{\mathrm{A}} - \mathbf{C}_{\mathrm{ext}}\left(T_{\mathrm{A}}\right)\right] + \mathbf{C}_{\mathrm{ext}}\left(T_{\mathrm{sky}}\right)$, where $\mathbf{C}_{\mathrm{ext}}$ is the contribution from the external isotropic thermal noise and the first two terms form the noise contribution due to ohmic losses of the antenna array [41]. Consequently, $\overline{\mathbf{b}\mathbf{b}^{\dagger}}$ leading to (16) is written as

$$\begin{aligned} \overline{\mathbf{b}\mathbf{b}^{\dagger}}\Big|_{T_{\mathrm{L}}=0} &= \mathbf{Q}\mathbf{S}\overline{\mathbf{a}_{\mathrm{s}}\mathbf{a}_{\mathrm{s}}^{\dagger}}\mathbf{S}^{\dagger}\mathbf{Q}^{\dagger} \\ &= \mathbf{Q}\mathbf{S}\begin{bmatrix} \mathbf{C}_{\mathrm{ext}}\left(T_{\mathrm{sky}}\right) - \mathbf{C}_{\mathrm{ext}}\left(T_{\mathrm{A}}\right) & \mathbf{0}_{2M\times 5M} \\ \mathbf{0}_{5M\times 2M} & \mathbf{0}_{5M\times 5M} \end{bmatrix}\mathbf{S}^{\dagger}\mathbf{Q}^{\dagger} \end{aligned} \tag{20}$$

to show that, when $T_{\mathrm{sky}} \neq T_{\mathrm{A}}$, the output of the networks is non-zero, resulting in a non-zero gain. In conclusion, the accuracy of detecting T_{sky} therefore relies on the accuracy of measuring T_{A}.

2) Non-Ideal Hybrids: Next, we used the 100-MHz S-parameters for Mini-Circuits JSPQW-100A+ hybrid in calculations depicted in Fig. 7. As we observed above, the optimum P_{H} depends on system components. Therefore, it is expected that in the final system a means of fine tuning P_{H} is required. In the calculation results depicted in Fig. 7(a) and (b), we include two identical phase shifters for each hybrid with adjustable phases $\Delta P_{\mathrm{H},1} = \Delta P_{\mathrm{H},2} = \Delta P_{\mathrm{H}}$ to determine that for the given system $\Delta P_{\mathrm{H}} \approx 98^{\circ}$ and $\Delta P_{\mathrm{H}} \approx 3^{\circ}$or 21.5° are required to minimize T_{rec} and $|T_{12}|$, respectively. Figs. 7(c) and (d) show the contours of constant gain magnitude, $|G_{12}|$, in response to a correlated input as functions of $S_{\mathrm{L},11}$ at $\Delta P_{\mathrm{H}} \approx 21.5^{\circ}$ and 3°. The maximum $|G_{12}|$ of ~ 3 is near the edges of the Smith chart with $|G_{12}| > 0$ throughout the Smith chart. $|G_{12}|$ can be increased further by increasing LNA $S_{\mathrm{L},21}$. From these figures, it is concluded that the network does not null the correlated input signal while nulling noise generated in the network circuit components. Note that not all values of $S_{\mathrm{L},11}$ in Figs. 7(c) and (d) realize nulls in $|T_{12}|$, and, therefore, not all $S_{\mathrm{L},11}$ identified in these figures may be desirable.

The contour plots of constant $|T_{12}|$ as functions of Γ_{opt} and $S_{\mathrm{L},11}$ are presented in Figs. 7(e) and (f) at $\Delta P_{\mathrm{H}} \approx 21.5^{\circ}$ and 3°. The two different phase settings result in two distinct contour plots. These calculations show that the phases, rather than magnitudes, of Γ_{opt} and $S_{\mathrm{L},11}$ are more significant to minimizing $|T_{12}|$. It is also observed that the decoupling condition of $\Delta P_{\mathrm{H}} \approx 3^{\circ}$ is less sensitive to Γ_{opt} and $S_{\mathrm{L},11}$ than the noise canceling $\Delta P_{\mathrm{H}} \approx 21.5^{\circ}$.

The possibility of adding a matching network to realize coincidental ΔP_{H} for the two nulls in the mutual coherence is explored in the next experiment whereby identical lossless single-stub matching networks are placed between the hybrids and LNAs. The matching network consists of a transmission line with a maximum length of 1λ that is manipulated in 0.1λ steps and a shunt capacitor stepped by 10 pF from 1 pF to 1 nF. Four results of this analysis, when the two nulls in the mutual coherence are located within 4° of each other, are shown in Fig. 8 where the resultant T_{12} as well as the realized Γ_{opt} and $S_{\mathrm{L},11}$ are presented.

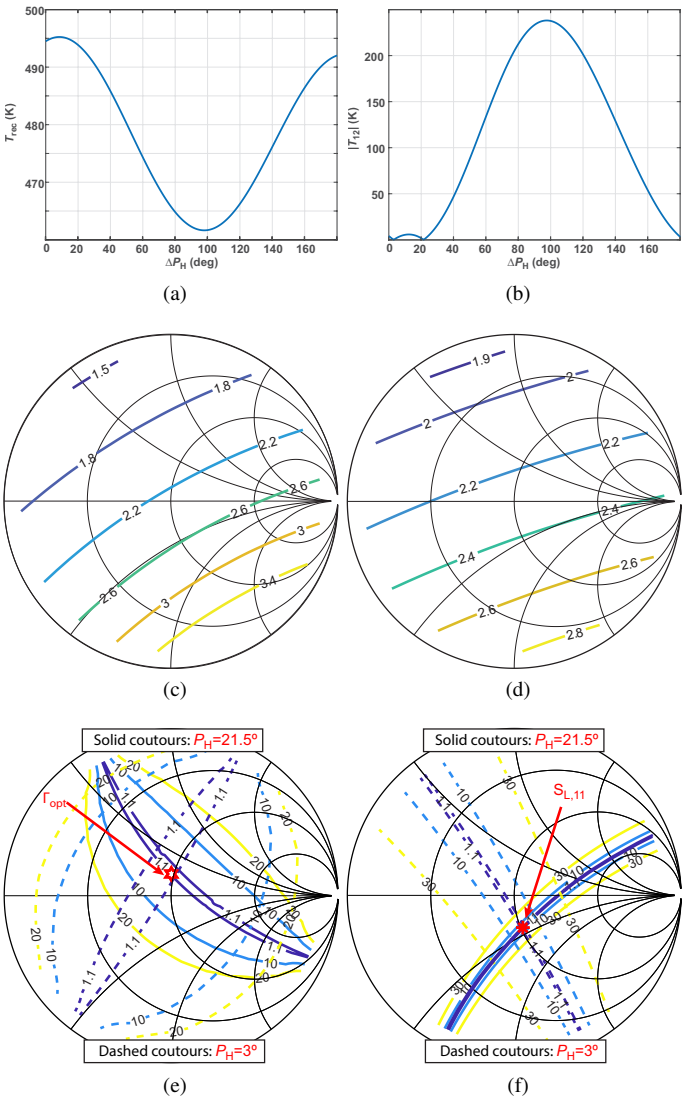

Fig. 7. Simulated a) $T_{\rm rec}$ and b) $|T_{12}|$ as functions of $\Delta P_{\rm H}$ with a non-ideal hybrid. The contour of constant gain $|G_{12}|$ as functions of $S_{\rm L,11}$ at $\Delta P_{\rm H} \approx 21.5°$and $P_{\rm H} \approx 3°$ are shown in c) and d), respectively. Also shown the contours of constant $|T_{12}|$ at $\Delta P_{\rm H} \approx 21.5°$and $3°$ as functions of e) $\Gamma_{\rm opt}$ and f) $S_{\rm L,11}$.

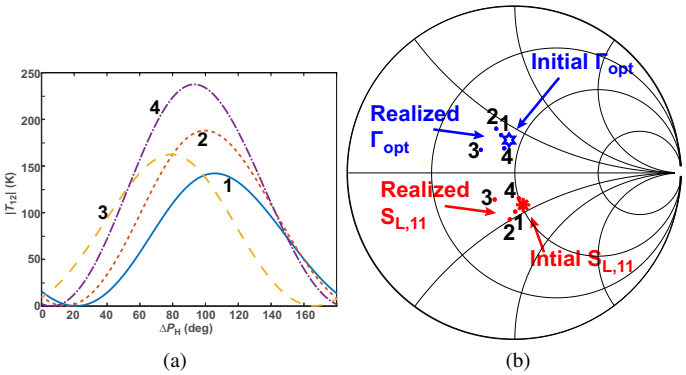

Fig. 8. a) Simulated $|T_{12}|$ with nearly coincidental zeros ($< 4°$ difference) in mutual coherence for lower sensitivity to $\Delta P_{\rm H}$. b) Locations 1 to 4 of realized $\Gamma_{\rm opt}$s and $S_{\rm L,11}$s corresponding to curves identified in a) with corresponding numbers. Also the initial $\Gamma_{\rm opt}$ and $S_{\rm L,11}$ of the LNAs are shown.

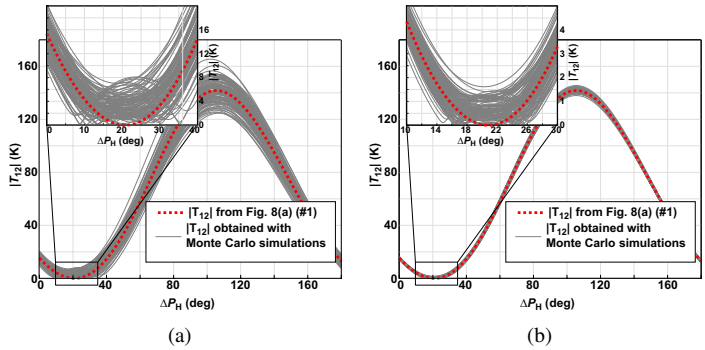

Fig. 9. Monte-Carlo simulation results of $|T_{12}|$ for the system configured as with the matching network realizing Location #1 of $S_{\rm L,11}$ and $\Gamma_{\rm opt}$ in Fig. 8(b). In the Monte-Carlo simulations, all S-parameters and $\Gamma_{\rm opt}$s are varied so that their maximum variations for each pair of the corresponding network components were limited to (a) 10% and (b) 2%.

3) Monte-Carlo Sensitivity Analysis: Sections IV-A1 and IV-A2 progressed from ideal networks to networks that included practical component models. When non-ideal hybrids were used, two identical phase shifters, with phases $\Delta P_{\rm H,1} = \Delta P_{\rm H,2} = \Delta P_{\rm H}$, were employed to adjust hybrid phases to realize nulls in mutual coherence. Section IV-A2 also investigated the possibility of using a matching network ahead of LNAs so as to make the two nulls nearly coincidental for relaxed sensitivity to hybrid phase errors. While these sections assumed that the arrays of antennas, hybrids, and LNAs were perfectly identical, in practical systems, this assumption will be violated. For example, imperfect replica-array absorber, fabrication inaccuracies, process variations in the LNA circuit components, and so on will cause the loss of identicalness and will require some degree of tuning and possibly sorting of parts to identify the most similar ones. This section analyzes the impact on $|T_{12}|$ of mismatch between the corresponding components of the network. Monte-Carlo simulations are used for this analysis whereby all magnitudes and phases of all S-parameters and the LNA $\Gamma_{\rm opt}$s are randomly varied within 5% and 1% of their original values, thereby creating maximum variations of 10% and 2%, respectively, between the corresponding components.

For these simulations, the network realizing Location #1 for $\Gamma_{\rm opt}$ and $S_{\rm L,11}$ in Fig. 8(b) was selected. The outcome of these simulations in Fig. 9 show that even the 2% variations in S-parameters and $\Gamma_{\rm opt}$s may result in the minimum of $|T_{12}|$ exceeding the 10s to 100s mK range required to discern the perturbations in the Cosmic Microwave Background. Although an analysis of the appropriate tuning is not the intent of this work, additional simulations were still performed to investigate the likelihood of tuning the minima in the $|T_{12}|$ curves below 10 mK. In these simulations, the phase shifter phases $\Delta P_{\rm H,1}$ and $\Delta P_{\rm H,2}$ were tuned independently. Fig. 10 shows the results of such analysis, where, for the case of the 10% variations, 34% of simulations returned minima in $|T_{12}|$ below 10 mK. This percentage increases to 52% when component mismatches are limited to 2%. These simulations suggest that two independently adjustable phase shifters and pre-selected components may be sufficient to null mutual coherence even when non-identical components are used.

B. Wideband interferometer

We next return to identical components and investigate the possibility of developing a wideband interferometer, such as, for example, would be used in cosmology instruments, by simulating the network in Fig. 1 in which the S-parameters of the antenna arrays are taken from calculations presented in [20], Mini-Circuits PMA2-43LN+ (biased with 60 mA current) is used for the LNA, and Mini-Circuits JSPQW-100A+ is used for the hybrid. This LNA

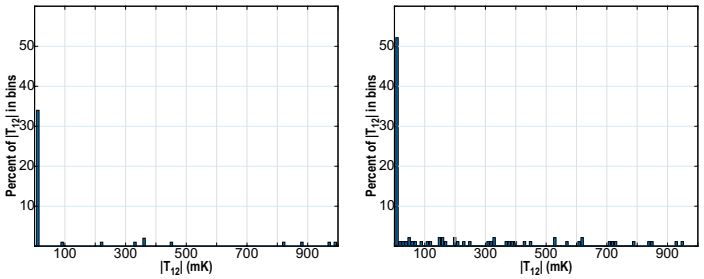

(a) 10% variations (b) 2% variations

Fig. 10. Histogram of $\min\{|T_{12}|\}$ distribution obtained with 100-iteration Monte-Carlo simulations with (a) 10% and (b) 2% variations between S-parameters and the LNA Γ_{opt}s of corresponding network components. In these simulations, ΔP_{H1} and ΔP_{H2} were independently swept. Each bin is 10 mK wide. Only bins below 1 K are shown.

was selected due to the availability of S-parameters and noise parameters in its datasheet. Still, the noise parameters are only given for frequencies above 800 MHz and the gain is low in the 50-to-100-MHz range. To rectify this, the noise parameters were linearly extrapolated to low frequencies as: $T_{\min} \approx T_0 \times 0.06 f_{\text{GHz}}$, $N \approx 0.34 - 0.3 \times f_{\text{GHz}}$, $Y_{\text{opt}} \approx (0.01 f_{\text{GHz}} + 0.004) - j0.005 f_{\text{GHz}}$, where $Y_{\text{opt}} = Z_0^{-1}(1 - \Gamma_{\text{opt}}) / (1 + \Gamma_{\text{opt}})$. All temperatures in $\mathbf{T}_{\text{PASS}}$ and T_{L} are set to 290 K. The S-parameters were used directly, as the low gain does not affect the results since the interferometer is assumed noiseless. In a practical implementation, an LNA developed specifically for this application would have sufficient gain to minimize the impact of the interferometer noise on the system performance.

The selected array is wideband and consists of two closely spaced short antenna dipoles over a ground plane for smooth response. The close spacing enables a response to the isotropic noise temperature component of the surrounding medium. As the result, the antennas are highly reflective. The $S_{\text{L},11}$ and Γ_{opt} of the selected LNA are also very reflective within the 50-to-100-MHz band. Numerical calculation results in Fig. 7 illustrate that large $|S_{\text{L},11}|$ and $|\Gamma_{\text{opt}}|$ are acceptable for minimizing $|T_{12}|$, although $|S_{\text{L},11}| \approx 0$ is preferred for the smooth trough in $|T_{12}|$ (see Fig. 5(d)) and $\Gamma_{\text{opt}} = S_{\text{H},11}$ results in the lowest T_{rec}.

Fig. 11 shows the results of the numerical analysis in which two identical ideal phase shifters (i.e. $\Delta P_{\text{H},1} = \Delta P_{\text{H},2} = \Delta P_{\text{H}}$) are inserted at the 90° terminals of the hybrids. The two phase-shifter phase curves in Fig. 11(a) correspond to the conditions of noise cancellation and decoupling. The required phase shifts to null mutual coherence exhibit monotonic behavior (see Fig. 11(a)). At low frequencies, the coupling is dominated by the hybrid (Fig. 11(b)). The decoupling phase-shifter phase is able to significantly increase the isolation between the LNAs beyond what is afforded by the antenna array itself. At higher frequencies, the array coupling dominates. The network is still able to null mutual coherence but at the cost of larger changes in the required phase shifter phase and higher sensitivity to the phase. When $S_{\text{L},11}$ and Γ_{opt} are reduced to nearly zero (1% of their original values), the optimum ΔP_{H} for the two conditions come close to each other and remain near-zero over most of the bandwidth, as shown in Fig. 11(c), indicating that with careful engineering of the LNA, wideband nulling in mutual coherence and coincidental nulls for less sensitivity to hybrid phase is likely possible.

V. Discussions

The inclusion of a replica array and 90° hybrids is shown to provide a means of nulling the mutual coherence at the output of a two-element interferometer. Two conditions for nulling are identified: decoupling and noise cancellation. Matching networks can be used to reduce the sensitivity of mutual coherence nulls to hybrid phase. The

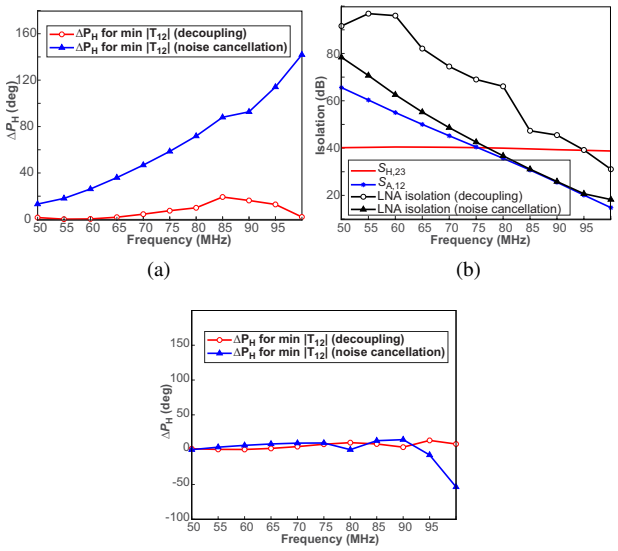

(a) (b)

(c)

Fig. 11. a) Extra phase from the phase shifters for minimum $|T_{12}|$ versus frequency; b) Simulated isolation between antennas ($S_{\text{A},12}$) and between the coupled ports of the hybrid ($S_{\text{H},23}$), as well as the effective isolation of the LNAs realized with the network when ΔP_{H} as in (a); and c) Extra phase from the phase shifters for minimum $|T_{12}|$ versus frequency when $S_{\text{L},11}$ and Γ_{opt} are near zero.

noise temperature of the interferometer is dominated by the ambient temperature of the replica array unless the latter is cooled. However, when nulling is achieved, the two-element interferometer becomes sensitive to even low-level correlated inputs such as isotropic noise temperature components of the surrounding medium.

For cosmology experiments in the 50-to-100-MHz range, the sky noise temperature $T_{\text{sky}} \approx 60\lambda^{2.55}$ [42], which corresponds to T_{sky} between 5800 and 1000 K. These values are larger than T_{rec}, the beam-equivalent receiver noise temperature of the interferometer, even without cooling (see Fig. 4), and are much larger in the limiting case when the replica array and the hybrids are cooled to nearly 0 K (see Figs. 2(a)-(c)). Note that for cosmology experiments, T_{rec} affects the integration time, and therefore keeping it below T_{sky} would result in minimum integration penalty. As a result, the proposed mutual-coupling canceler is of potential interest for radio cosmology.

VI. Conclusion

This paper investigated the use of a previously-proposed self-interference canceler on the noise performance of two-element phased arrays and interferometers. In this work, the canceler acts as a mutual-coupling canceler. When used in phased arrays, the canceler makes LNA noise matching independent of the beamformer coefficients but increases the beam-equivalent noise temperature by the physical temperature of the canceler. In an interferometric applications, the addition of the canceler nulls mutual coherence in the output of the interferometer while realizing gain in response to correlated inputs to the antennas. It was shown that the accuracy of detecting the noise temperature of a uniform sky, T_{sky}, with the proposed network relies on the accuracy of measuring its physical temperature. With non-ideal, realistic, and wideband hybrid and antenna models, the low input reflection coefficient and Γ_{opt} of LNAs realize two nulls in the mutual coherence that are nearly coincidental even without additional matching networks or means of tuning the hybrid phases. However, when there are practical mismatches in network components, Monte-Carlo analysis demonstrated that to lower mutual coherence, there is a need for adjusting phases of each hybrid independently.

The analysis in this work employed a general framework, which can also be used for a large variety of other networks, such as an implementation-ready network of the two-element interferometer that includes tuning networks, additional amplifiers, any cables, and a non-ideal interferometer.

Future work will include thorough analysis of the effect of mismatches between the system components in a wideband system. The proposed framework for analyzing noise will be used to determine the advantageous combinations of the component S-parameters that are both realizable and able to create wideband nulls in mutual coherence. This will lead to identifying the minimum sufficient set of variable/tunable network parameters required to null mutual coherence even with not-exactly-identical components and to ultimately enable the experimental validation of the results of this work.

REFERENCES

[1] J. A. de Zwart *et al.*, "Design of a SENSE-optimized high-sensitivity MRI receive coil for brain imaging," *Magn. Resonance in Med.*, vol. 47, no. 6, pp. 1218–1227, June 2002.

[2] G. Krieger, N. Gebert, and A. Moreira, "Multidimensional waveform encoding: A new digital beamforming technique for synthetic aperture radar remote sensing," *IEEE Trans. Geosci. Remote Sens.*, vol. 46, no. 1, pp. 31–46, Jan. 2008.

[3] T. Heath *et al.*, "Simultaneous, multi-frequency synchronous oscillator antenna," in *IEEE Military Commun. Conf.*, San Diego, 16-19 Nov. 2008, pp. 1–7.

[4] P. Dewdney *et al.*, "The Square Kilometre Array," *Proc. IEEE*, vol. 97, no. 8, pp. 1482–1496, Aug. 2009.

[5] R. Zhang *et al.*, "Multi-antenna based spectrum sensing for cognitive radios: A GLRT approach," *IEEE Trans. Commun.*, vol. 58, no. 1, pp. 84–88, Jan. 2010.

[6] E. Brookner, "Never ending saga of phased array breakthroughs," in *IEEE Int. Symp. Phased Array Syst. Tech. (ARRAY)*, Waltham, MA, 12-15 Oct. 2010, pp. 61–73.

[7] D. Heo and K. F. Warnick, "Integrated eight element Ku band transmit/receive beamformer chipset for low-cost commercial phased array antennas," in *IEEE Int. Symp. Phased Array Syst. Tech. (ARRAY)*, Waltham, MA, 12-15 Oct. 2010, pp. 653–659.

[8] A. Natarajan *et al.*, "A fully-integrated 16-element phased-array receiver in SiGe BiCMOS for 60-GHz communications," *IEEE J. Solid-State Circuits*, vol. 46, no. 5, pp. 1059–1075, May 2011.

[9] O. Inac *et al.*, "A 90-100-GHz phased-array transmit/receive silicon RFIC module with built-in self-test," *IEEE Trans. Microw. Theory Techn.*, vol. 61, no. 10, pp. 3774–3782, Oct. 2013.

[10] T. S. Rappaport *et al.*, "Wireless communications and applications above 100 GHz: Opportunities and challenges for 6G and beyond," *IEEE Access*, vol. 7, pp. 78 729–78 757, 2019.

[11] N. Rajatheva *et al.*, "White paper on broadband connectivity in 6G." [Online]. Available: https://arxiv.org/pdf/2004.14247.pdf

[12] W.-C. Liao *et al.*, "Antenna mutual coupling effects in highly integrated transmitter arrays," in *Eur. Conf. Antennas Propag. (EuCAP)*, 2020, pp. 1–4.

[13] A. P. Chippendale, D. B. Hayman, and S. G. Hay, "Measuring noise temperatures of phased-array antennas for astronomy at CSIRO," *Publications Astronomical Soc. Australia*, vol. 31, pp. 1–14, Jan. 2014.

[14] Y. Wang *et al.*, "Δ-Σ noise-shaping in 2-D space-time for wideband antenna array receivers," *IEEE Trans. Circuits Syst. I*, vol. 66, no. 2, pp. 569–582, 2018.

[15] A. H. Aljuhani *et al.*, "A 256-element Ku-band polarization agile SATCOM receive phased array with wide-angle scanning and high polarization purity," *IEEE Trans. Microw. Theory Techn.*, vol. 69, no. 5, pp. 2609–2628, 2021.

[16] H. Zhao *et al.*, "A broadband multistage self-interference canceller for full-duplex MIMO radios," *IEEE Trans. Microw. Theory Techn.*, vol. 69, no. 4, pp. 2253–2266, 2021.

[17] R. D. Beyers and D. I. L. de Villiers, "A general isolation network for N-way power combiners/dividers," in *IEEE Int. Microw. Symp.*, 2015, pp. 1–4.

[18] R. A. Monsalve *et al.*, "Calibration of the EDGES high-band receiver to observe the global 21 cm signature from the epoch of reionization," *The Astrophysical J.*, vol. 835, no. 1, p. 49, Jan. 2017.

[19] T. Venumadhav *et al.*, "A practical theorem on using interferometry to measure the global 21 cm signal," *The Astrophysical J.*, vol. 826, no. 2, p. 116, jul 2016. [Online]. Available: https://doi.org/10.3847/0004-637x/826/2/116

[20] A. T. Sutinjo *et al.*, "Design equations for closely spaced two-element interferometer for radio cosmology," *URSI Radio Sci. Lett.*, vol. 2, pp. 1–5, 2020.

[21] J. Andersen and H. Rasmussen, "Decoupling and descattering networks for antennas," *IEEE Trans. Antennas Propag.*, vol. 24, no. 6, pp. 841–846, 1976.

[22] H. J. Chaloupka and X. Wang, "Novel approach for diversity and MIMO antennas at small mobile platforms," in *Int. Symp. Pers., Indoor, Mobile Radio Commun.*, 2004, pp. 637–642.

[23] J. Weber *et al.*, "Miniaturized antenna arrays using decoupling networks with realistic elements," *IEEE Trans. Microw. Theory Techn.*, vol. 54, no. 6, pp. 2733–2740, 2006.

[24] A. Diallo *et al.*, "Study and reduction of the mutual coupling between two mobile phone PIFAs operating in the DCS1800 and UMTS bands," *IEEE Trans. Antennas Propag.*, vol. 54, no. 11, pp. 3063–3074, 2006.

[25] C. Volmer *et al.*, "An eigen-analysis of compact antenna arrays and its application to port decoupling," *IEEE Trans. Antennas Propag.*, vol. 56, no. 2, pp. 360–370, 2008.

[26] K. Warnick and M. Jensen, "Optimal noise matching for mutually coupled arrays," *IEEE Trans. Antennas Propag.*, vol. 55, no. 6, pp. 1726–1731, June 2007.

[27] K. Warnick *et al.*, "Minimizing the noise penalty due to mutual coupling for a receiving array," *IEEE Trans. Antennas Propag.*, vol. 57, no. 6, pp. 1634–1644, June 2009.

[28] L. Belostotski *et al.*, "Low noise amplifier design considerations for use in antenna arrays," *IEEE Trans. Antennas Propag.*, vol. 63, no. 6, pp. 2508–2520, June 2015.

[29] M. V. Ivashina, R. Maaskant, and B. Woestenburg, "Equivalent system representation to model the beam sensitivity of receiving antenna arrays," *IEEE Antennas Wireless Propag. Lett.*, vol. 7, pp. 733–737, 2008.

[30] D. C. X. Ung *et al.*, "Noise temperature of phased array radio telescope: The Murchison Widefield Array and the Engineering Development Array," *IEEE Trans. Antennas Propag.*, vol. 68, no. 7, pp. 5395–5404, 2020.

[31] C. Findeklee, "Array noise matching – generalization, proof and analogy to power matching," *IEEE Trans. Antennas Propag.*, vol. 59, no. 2, pp. 452–459, Feb. 2011.

[32] H. Bosma, "On the theory of linear noisy systems," *Philips Res. Rep., Supplement*, no. 10, pp. 1–189, 1967.

[33] S. Wedge and D. Rutledge, "Noise waves and passive linear multiports," *IEEE Microw. Guided Wave Lett.*, vol. 1, no. 5, pp. 117–119, May 1991.

[34] S. Wedge and D. Rutledge, "Wave techniques for noise modeling and measurement," *IEEE Trans. Microw. Theory Techn.*, vol. 40, no. 11, pp. 2004–2012, Nov. 1992.

[35] J. Lange, "Noise characterization of linear twoports in terms of invariant parameters," *IEEE J. Solid-State Circuits*, vol. 2, no. 2, pp. 37–40, June 1967.

[36] L. Belostotski, "On the number of noise parameters for analyses of circuits with MOSFETs," *IEEE Trans. Microw. Theory Techn.*, vol. 59, no. 4, pp. 877–881, Apr. 2011.

[37] K. F. Warnick *et al.*, "Unified definitions of efficiencies and system noise temperature for receiving antenna arrays," *IEEE Trans. Antennas Propag.*, vol. 58, no. 6, pp. 2121–2125, 2010.

[38] R. Ali *et al.*, "Impact of bandwidth on antenna-array noise matching," *Electron. Lett.*, vol. 57, no. 4, pp. 158–160, 2021.

[39] R. Maaskant and E. Woestenburg, "Applying the active antenna impedance to achieve noise match in receiving array antennas," in *Int. Symp. Antennas Propag.*, Honolulu, 9–15 June 2007, pp. 5889–5892.

[40] S. de Silva, M. Okoniewski, and L. Belostotski, "Antenna-array network model," *IEEE Trans. Antennas Propag.*, vol. 68, no. 7, pp. 5387–5394, 2020.

[41] K. Warnick and B. Jeffs, "Efficiencies and system temperature for a beamforming array," *IEEE Antennas Wireless Propag. Lett.*, vol. 7, pp. 565–568, July 2008.

[42] R. J. Nijboer, M. Pandey-Pommier, and A. G. de Bruyn, "LOFAR imaging capabilities and system sensitivity," 2013. [Online]. Available: https://arxiv.org/abs/1308.4267

Leonid Belostotski (Senior Member, IEEE) received the B.Sc. and M.Sc. degrees in electrical engineering from the University of Alberta, Edmonton, AB, Canada, in 1997 and 2000, respectively, and the Ph.D. degree from the University of Calgary, Calgary, AB, Canada, in 2007. He was a RF Engineer with Murandi Communications Ltd., Calgary, from 2001 to 2004. He is currently a Professor with the University of Calgary and the Canada Research Chair in high-sensitivity radiometers and receivers. His current research interests include RF and mixed-signal ICs, high-sensitivity receiver systems, antenna arrays, and terahertz systems. He was a recipient of the Outstanding Student Designer Award from Analog Devices Inc., in 2007, and the IEEE Microwave Theory and Techniques-11 Contest on Creativity and Originality in Microwave Measurements, in 2008. He serves as the IEEE Southern Alberta Solid-State, Circuits and Circuits and Systems Chapter's Chair. He served as an Associate Editor for the IEEE TRANSACTIONS ON INSTRUMENTATION AND MEASUREMENT. He is the Editor-in-Chief for the IEEE SOLID-STATE CIRCUITS MAGAZINE.

Adrian T. Sutinjo (Senior Member 2015) received the B.S.E.E. degree from Iowa State University, Ames, IA, USA, in 1995, the M.S.E.E. degree from the Missouri University of Science and Technology, Rolla, MO, USA, in 1997, and the Ph.D. degree in electrical engineering from the University of Calgary, Calgary, AB, Canada, in 2009. From 1997 to 2004, he was an RF Engineer with Motorola, Schaumburg, IL, USA, and with Murandi Communications Ltd., Calgary. He is currently a Senior Lecturer with the School of Electrical Engineering, Computing and Mathematics, Curtin University, Perth, WA, Australia. He has been with the International Centre for Radio Astronomy Research/Curtin Institute of Radio Astronomy, Curtin University, Bentley, WA, Australia, since 2012. His current research interests include antennas, RF and microwave engineering, electromagnetics, and radio astronomy engineering.

Ravi Subrahmanyan received the B.Tech degree in Electrical Engineering from the Indian Institute of Technology, Madras, India, in 1983 and the Ph.D. degree in astronomy from the Physics department of the Indian Institute of Science, Bangalore, India, in 1990. He is with Space & Astronomy, CSIRO, Australia.

Soumyajit Mandal (S'01--M'09--SM'14) received the B.Tech. degree from the Indian Institute of Technology (IIT) Kharagpur, India, in 2002, and the S.M. and Ph.D. degrees in electrical engineering from the Massachusetts Institute of Technology (MIT), Cambridge, MA, USA, in 2004 and 2009, respectively.

He was a Research Scientist with Schlumberger-Doll Research, Cambridge (2010 - 2014), an Assistant Professor with the Department of Electrical Engineering and Computer Science, Case Western Reserve University, Cleveland, OH, USA (2014 – 2019), and an Associate Professor with the Department of Electrical and Computer Engineering, University of Florida, Gainesville, FL, USA (2019 – 2021). He is currently a Senior Engineer in the Instrumentation Division at Brookhaven National Laboratory, Upton, NY, USA. He has over 150 publications in peer-reviewed journals and conferences and has been awarded 26 patents. His research interests include analog and biological computation, magnetic resonance sensors, low-power analog and RF circuits, and precision instrumentation for various biomedical and sensor interface applications. He was a recipient of the President of India Gold Medal in 2002, the MIT Microsystems Technology Laboratories (MTL) Doctoral Dissertation Award in 2009, the T. Keith Glennan Fellowship in 2016, and the IIT Kharagpur Young Alumni Achiever Award in 2018.

Arjuna Madanayake is an Associate Professor at the Dept. of Electrical and Computer Engineering (ECE) at Florida International University (FIU), Miami, Florida. He as awarded the Ph.D. and M.Sc. degrees both in Electrical Engineering from the University of Calgary, AB,Canada, in 2008 and 2004, respectively. He completed the B.Sc. [Eng] in Electronic and Telecommunication Engineering- passing with First Class Honors - from the University of Moratuwa, Sri Lanka, in 2002. Dr. Madanayake has research interests spanning signal processing, wireless communications, analog and digital circuits, RF systems, antenna arrays, FPGA systems, radar and electronic warfare, fast algorithms and VLSI, analog computing, radio astronomy instrumentation, 5G/6G mm-wave systems, advanced spectrum, blockchain applications for spectrum, RF-machine learning, AI accelerators for 6G, and software defined radio (SDR). He leads the RF, Analog and Digital (RAND) Lab for Advanced Signal Processing Circuits (ASPC) where his research has been recently supported by multiple grants from NSF, ONR, NASA, NIH and DARPA.